BULK AMORPHOUS AND NANOCRYSTALLINE Al-BASED ALLOYS WITH HIGH STRENGTH

Tsuyoshi MASUMOTO* and Akihisa INOUE**

*Electric Magnetic Institute, Sendai
**Institute Materials Research, Tohoku University, Sendai 980-8577, Japan

ABSTRACT A new type of hig-strength Al-based alloys with an amorphous or nanoscale compound plus Al phase have been developed in Al-R-LM and Al-EM-LM (R=rare earth metal, EM=IV-VI group metals, LM=VII and VIII group metals) systems by the use of rapid solidification and powder metallurgy (P/M) techniques. The high-strength bulk alloys were synthesized by the P/M process of the formation of amorphous alloy powder, followed by warm extrusion at temperatures well below crystallization temperature (T_x) for the Am alloys, near the T_x for the nanoscale compound+Al alloys. The highest strength reaches about 1200 MPa for the former bulk alloys and 1000 MPa for the latter bulk alloys. The high strength values are promising for future application of the nonequilibrium Al-based alloys.

1. INTRODUCTION

Since the first synthesis of an amorphous phase in Au-Si system by rapid solidification in 1960[1], a great number of amorphous alloys have been synthesized by various preparation methods of rapid quenching from liquid or vapor and solid-state reactions[2-4]. However, the maximum thickness of the resulting amorphous alloys had usually been limited to less than 100 μm for the subsequent three decades. The limitation of the maximum sample thickness has prevented a wide extension of application fields of amorphous alloys. Consequently, great efforts have been devoted to prepare a bulk amorphous alloy from amorphous alloy powder by using various techniques of warm pressing, warm extrusion and explosive compaction etc.[5,6]. However, there have been no successful data on the production of a bulk amorphous alloy having the same mechanical, chemical and soft magnetic properties as those for the corresponding melt-spun amorphous alloy ribbons. Owing to the poor engineering properties for the consolidated bulk amorphous alloys, the bulk amorphous alloys had not gained any practical applications. Under such a blocking situation, amorphous alloys with much higher glass-forming ability have been found[7-9] in a number of alloy systems such as Mg-Ln-TM, Ln-Al-TM, Zr-Al-TM, Zr-Ti-TM-Be, Zr-(Ti,Nb,Pd)-Al-TM, Pd-Cu-Ni-P, Fe-(Al,Ga)-(P,C,B,Si) and (Fe,Co,Ni)-(Zr,Hf,Nb)-B (Ln=lanthanide metal, TM=transition metal). The use of the new multicomponent alloy systems has enabled the production of bulk amorphous alloys within a thickness range up to about 75 mm by conventional solidification methods. These bulk amorphous alloys exhibit the same mechanical and magnetic properties as those for the corresponding melt-spun amorphous alloy ribbons and have been expected to be used as a new engineering material.

In addition to the above-described development of bulk amorphous alloys, a number of trials to produce a bulk nanocrystalline alloy by various consolidation techniques have been carried out for the last three decades. As main raw materials to produce bulk nanogranular alloys, one can list up melt-spun alloy ribbon, atomized alloy powder, vapor condensated powder and mechanically alloyed powder which have metastable structures consisting of amorphous, quasicrystalline and nanocrystalline phases. The subsequent condensatin of these raw materials into a bulk form gives rise to a structural change into various nanogranular structures. These bulk nanogranular alloys exhibit good mechanical and physical properties and have already been used as engineering materials. This review is intended to present recent progress of bulk nanogranular alloys prepared by warm consolidation of amorphous, amorphous plus nanocrystalline and nanoquasicrystalline alloys obtained by rapid solidification as well as of bulk amorphous alloys prepared by various casting processes and warm consolidation. The reason for the limitation of the solidified alloys from liquid is due to the ease of mass production of bulk amorphous alloys with a larger scale as compared with vapor deposited powder and mechanically alloyed powder.

2. HISTORY OF Al-BASED AMORPHOUS ALLOYS

It is very difficult to obtain a bulk nanogranular structure in Al-based alloys containing a large amount of solute elements by the use of direct solidification methods. We have noticed that the use of Al-based amorphous alloys as a precursor to prepare a nanogranular structure is useful for the production of bulk nanogranular alloys exhibiting good mechanical properties. Consequently, the progress of the development of Al-based amorphous alloys themselves is firstly reviewed.

The formation of Al-based amorphous alloys by liquid quenching was first tried in binary systems of Al-metalloid and Al-transitin metal (M). As a result, it was found in Al-Si[10], Al-Ge[11] and Al-M(M=Cu[12], Ni[13], Cr[14] or Pd[15]) alloys that a coexistent structure of amorphous and crystalline phase is formed only near the holes in their thin foils prepared by the gun quenching technique in which the cooling rate is higher than that for the melt spinning method. However, no amorphous phase without crystallinity was prepared by melt spinning as well as by the gun- and piston-anvil methods. The first formation of an amorphous single phase in Al-based alloys containing more than 50 at% Al was achieved in 1981 for Al-Fe-B and Al-Co-B ternary alloys[16]. However, these amorphous alloys are extremely brittle and hence have not attracted strong attention. Subsequently, an amorphous phase was found in melt-spun Al-Fe-Si Al-Fe-Ge and Al-Mn-Si alloys[17], but they were also brittle, similar to the Al-(Fe or Co)-B amorphous alloys. It was believed from these data that the brittleness might be an inherent property for Al-based amorphous alloys. However, in 1987, an amorphous phase with good bending ductility was discovered by Inoue et al.[18] to be formed at compositions above about 80 at% Al in Al-Ni-Si and Al-Ni-Ge systems. Since the discovery, ductile Al-based amorphous alloys have successively been found in a number of ternary alloys consisting of Al-early transition metal(EM)-late transition metal(LM)[19], which are exemplified for Al-Zr-Cu, Al-Zr-Ni and Al-Nb-Ni systems. These were followed by Al-rare earth metal(R)-LM ternary alloys[20] in which the EM is substituted by Ln, and then Al-Ln binary alloys without M elements[21]. The review on the formation, structure and properties of Al-based amorphous alloys will be focussed on Al-EM-LM and Al-Re-LM ternary alloys without metalloid elements because higher glass-forming ability and better mechanical strength have been obtained in their ternary alloys.

3. Al-EM-LM AMORPHOUS ALLOYS

3.1 Amorphous Alloy Systems

Fugure 1 shows the effect of EM (EM=Ti, Zr, Hf, V, Nb, Ta, Cr, Mo or W) elements on the glass formation of $Al_{70}Fe_{20}M_{10}$, $Al_{70}Co_{20}M_{10}$ and $Al_{70}Cu_{20}M_{10}$ alloys by melt spinning. The effectiveness of the M elements to form an amorphous phase is the greatest for Zr and Hf and decreases in the order of Ti > V > Mo > Nb > Cr > Ta. No amophous phase was observed in the Al-based alloys containing W. Thus, the alloys are composed of the LM of Fe, Co, Ni and Cu, and the EM of Ti, Zr, Hf etc. and can form metal-metal type Al-based amorphous structures. It is also noteworthy that the formation of the amorphous alloys extends over rather wide compositional ranges around the $Al_7(LM)_2(EM)_1$ compositions. For instance, the formation range extends from 5 to 35 %Cu and 5 to 15 %V for the Al-Cu-V system[22] and from 10 to 30 %Ni and 5 to 20 %Zr for the Al-Ni-Zr system[19].

M	Ti	Zr	Hf	V	Nb	Ta	Cr	Mo	W
$Al_{70}Fe_{20}M_{10}$	●	○	○	●	●	●	●	●	●
$Al_{70}Co_{20}M_{10}$	○	○	○	●	●	●	●	●	●
$Al_{70}Ni_{20}M_{10}$	○	○	○	○	○	◑	◑	○	●
$Al_{70}Cu_{20}M_{10}$	◑	○	○	○	●	●	◑	○	●

○ Amorphous ◑ Amorphous + crystalline ● Crystalline

Fig. 1 Effect of the early transition M metals on the glass formation of $Al_{70}Fe_{20}M_{10}$, $Al_{70}Co_{20}M_{10}$ and $Al_{70}Cu_{20}M_{10}$ (M=Ti, Zr, Hf, V, Nb, Ta, Cr, Mo or W) alloys by melt spinning.

The reason for the glass formation of the metal-metal type Al-based alloys is briefly discussed. The amorphous alloys are composed of Al, LM and EM. Furthermore, most of the binary alloys consisting of LM and EM except Al can be amorphized by melt spinning as exemplified for Fe-(Zr, or Hf), Co-(Ti, Zr of Hf), Ni-(Ti, Zr or Hf) and Cu-(Zr or Hf)[33]. It has generally been known[23] that the amorphization of alloys is closely related to the ratio of T_g/T_m and the larger the ratio the higher is the glass-forming tendency. Although the T_m of Al-Cu alloys decreases with increasing Cu content in the range below 17.3 %, T_m of the other Al-M binary alloys rises rapidly with increasing M content[24]. However, by the presence of the LM and EM, the rise of Tm of the Al-based ternary alloys is thought to be significantly depressed because many eutectic points exist in the binary alloys of LM and EM[34]. In addition, a number of intermetallic compounds are formed in Al-M alloys as well as in EM-LM alloys[24]. It is therefore presumed that the attractive interaction among the constituent elements is significantly enhanced by adding the EM to the Al-LM binary alloys, leading to the increase in the viscosity of supercooled liquid and its temperature dependence which causes the enhancement of glass formation. The decrease of T_m and the increase of the attractive interaction among the constituent elements by the coexistence of Al, LM and EM appear to be dominant factors for the amorphization of the present metal-metal type amorphous alloys. On the other hand, the reason why no amorphization was observed in the alloy systems such as Al-(Fe, Co, Ni or Cu)-W and Al-(Fe or Co)-(V, Nb, Ta, Cr, Mo or W) etc. is probably because of the weak attrcative interaction between LM and EM, as is evidenced from the existence of a wide solid solubility range in the binary alloys of LM and EM[24].

3.2 Thermal and Mechanical Properties of Melt-spun Al-based Amorphous Alloy Ribbons

Figure 2 shows the changes in T_x and H_v of the amorphous $Al_{70}Fe_{20}M_{10}$, $Al_{70}Co_{20}M_{10}$, $Al_{70}Ni_{20}M_{10}$ and $Al_{70}Cu_{20}M_{10}$ (M=Ti, Zr, Hf, V, Nb or Mo) lloys with M element. Considering the $Al_{70}Ni_{20}M_{10}$ alloys where the amorphization is achieved for various kinds of M elements, the values of T_x and H_v in the same group number tend to increase with increasing atomic number while no systematic change in these values with group number is observed. Additionally, T_x and H_v decrease in the order of Fe > Co > Ni > Cu in $Al_{70}Fe_{20}M_{10}$, $Al_{70}Co_{20}M_{10}$, $Al_{70}Ni_{20}M_{10}$ and $Al_{70}Cu_{20}M_{10}$ amorphous alloys, sugesting that the bonding nature between Fe, Co, Ni or Cu and the other constituent elements decreases in the same order. This order agrees with the result[24] that the T_g of Al-rich Al-EM and Al-LM compounds and EM-LM compounds decrease in the order of Fe > Co > Ni > Cu. The highest values

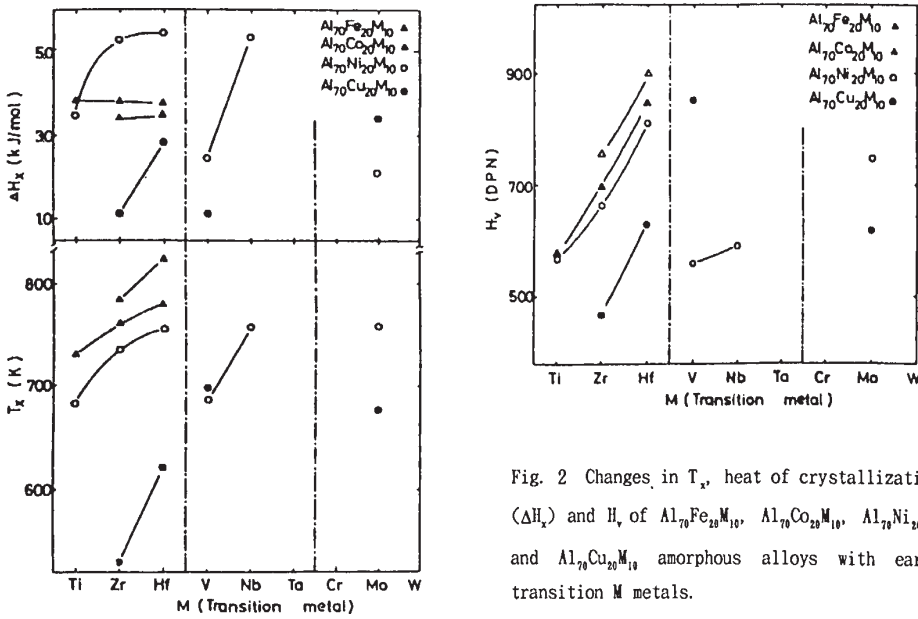

Fig. 2 Changes in T_x, heat of crystallization (ΔH_x) and H_v of $Al_{70}Fe_{20}M_{10}$, $Al_{70}Co_{20}M_{10}$, $Al_{70}Ni_{20}M_{10}$ and $Al_{70}Cu_{20}M_{10}$ amorphous alloys with early transition M metals.

of T_x and H_v reach 825 K and 900, respectively, for $Al_{70}Fe_{20}Hf_{10}$, being comparable to those[3] for Fe-, Co- and Ni-based amorphous alloys.

In the Al-EM-LM amorphous alloys, the Al-Ni-Zr and Al-Ni-Hf alloys were found to be alloy systems with high GFA and the easy amorphization enabled us to examine the compositional dependence of σ_f and Young's modulus (E). As an example, Fig. 3 shows the compositional range in which amorphous Al-Ni-Zr phase is formed by melt spinning, along with the data of T_x and bending ductility of the amorphous alloys. The glass formation is in the range of 8 and 32 %Ni and 3 to 18 %Zr. It is notable that the amorphous alloys containing more than about 80 %Al can be completely bent through 180 degrees without fracture and no appreciable cracking is observed even at the severely deformed area. The ductility of the Al-Ni-Zr amorphous alloys is strongly dependent on the alloy composition and there is a clear tendency that the higher the Al content the higher is the ductility. On the other hand, T_x increases with decreasing Al content and shows the highest value (790 K) at 30 %Ni and 10 %Zr.

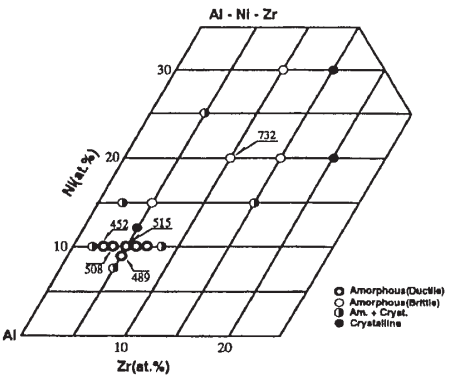

Fig. 3 Composition range and T_x in melt-spun Al-Ni-Zr alloys.

The σ_f, E, H_v and T_x of Al-Ni-Zr and Al-Ni-Hf amorphous alloys are summarized in Table 1, where the data of tensile fracture strain ($\varepsilon_f = \sigma_f/E$) and compressive strain ($\varepsilon_y \fallingdotseq 9.8H_v/3E$) are based on the fact that amorphous alloys exhibit little work-hardening and thus the compressive yield strength is related by $\sigma_y \fallingdotseq 9.8H_v/3$[25]. It can be seen in the table that the decrease in Al content gives rise to the increase from 580 to 800 MPa for σ_f, 50 to 80 GPa for E, 2740 to 3330 MPa for H_v and 452 to 515 K for T_x, indicating a similar compositional dependence in σ_f, E, H_v and T_x. Additionally, Fig. 4 shows the correlation between E and the properties T_x, σ_f and H_v for Al-Ni-Zr amorphous alloys. The three properties of T_x, σ_f or H_v can be empirically expressed by the following approximate equations: $\varepsilon_f = \sigma_f/E \fallingdotseq 0.011$ and $\varepsilon_y \fallingdotseq 9.8H_v/3E \fallingdotseq 0.015$. The fracture behavior for the Al-Ni-Zr amorphous alloys is the same as those reported previously[26] for the other ductile amorphous alloys.

Table 1 Mechanical properties, thermal stability and electrical resistivity of Al-Ni-Zr, Al-Ni-Hf and Al-Ni-Nb amorphous.

Alloy (at%)	T_x (K)	σ_f (MPa)	E (MPa)	H_v (DPN)	$\rho_{R.T.}$ ($\mu\Omega$ cm)	$1/\rho_{R.T.}$ ($d\rho/dT$) (K^{-1})
$Al_{87}Zr_3Ni_{10}$	452	580	50000	280	–	–
$Al_{86}Zr_4Ni_{10}$	508	680	65700	330	340	5.23×10^{-5}
$Al_{86}Zr_5Ni_9$	489	750	72500	300	200	0.74×10^{-5}
$Al_{85}Zr_5Ni_{10}$	515	800	80400	340	460	0.97×10^{-5}
$Al_{85}Hf_5Ni_{10}$	560	730	75800	350	380	3.25×10^{-5}
$Al_{85}Nb_5Ni_{10}$	460	–	–	280	280	0.43×10^{-5}

4. Al-RARE EARTH METAL (R)-TRANSITION METAL (M) AMORPHOUS ALLOYS

4.1 Formation Ranges[20]

Figure 5 shows the compositional ranges in which amorphous Al-Y-M, Al-La-M and Al-Cr-M (M=Fe, Co, Ni or Cu) phases are formed by melt spinning. The formation ranges of Al-Y-M and Al-Ce-M amorphous alloys are the widest for the Al-Y-Ni and Al-Ce-Ni systems. No distinct difference is seen among the other three alloys in the Al-Y-M and Al-Ce-M systems, while those

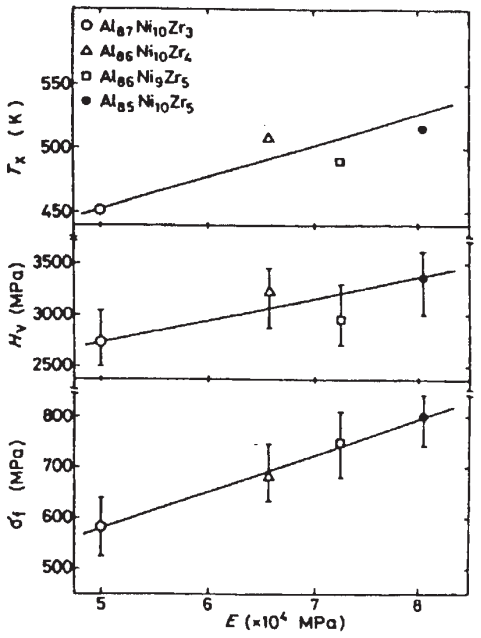

Fig. 4 Correlation between Young's modulus (E) and T_x, tensile fracture strength (σ_f) or H_v for Al-Ni-Zr amorphous alloys.

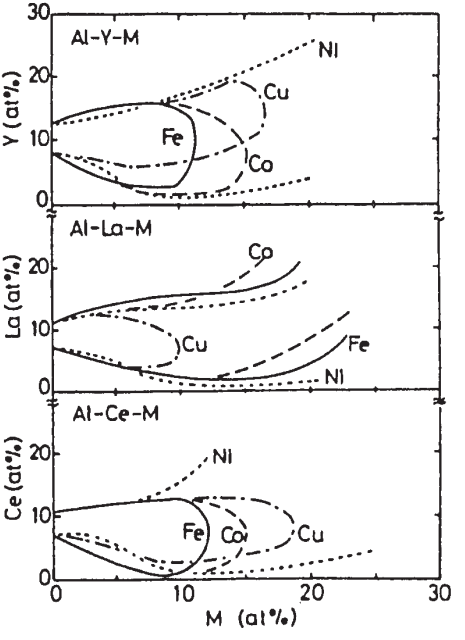

Fig. 5 Compositional ranges for formation of an amorphous phase in Al-Y-M, Al-La-M and Al-Ce-M (M=Fe, Co, Ni or Cu) systems.

for the Al-La-M amorphous alloys are the narrowest for the Al-La-Cu system and much wider for the other Al-La-(Fe, Co, Ni) systems. Accordingly, the effectiveness of M elements on the compositional range for formation of the Al-based amorphous alloys is the greatest for Ni, followed by Fe, Co and then Cu. These amorphous alloys containing more than about 80 %Al can be completely bent by 180 degrees without fracture, and no appreciable crack is observed even in the severely deformed area. The ductility of the Al-R-M amorphous alloys is strongly dependent on alloy composition and there is a clear tendency for the ductility to increase with increasing Al content.

4.2 Thermal Stability[20, 27]

In order to clarify the compositional dependence of thermal stability for the Al-Y-M, Al-La-M and Al-Ce-M amorphous alloys, we plotted T_x as a function of M (M=Fe, Co, Ni or Cu) or R (R=Y, La or Ce) content in Fig. 6. T_x values of the Al-based alloys without Cu element have a distinct compositional dependence and increase significantly with an increase of Fe, Co, Ni, Y, La or Ce content, i.e., from 528 to 724 K for $Al_{90-x}Y_{10}M_x$, 544 to 793 K for $Al_{90-x}La_{10}M_x$, 500 to 730 K for $Al_{90-x}Ce_xM_{10}$, 414 to 750 K for $Al_{90-x}Y_xM_{10}$, 486 to 740 K for $Al_{90-x}La_xM_{10}$ and 402 to 620 K for $Al_{90-x}Ce_xM_{10}$. There is no distinguishable difference in the compositional dependence of T_x among the Al-Y-M, Al-La-M and Al-Ce-M alloys. The effect of M elements on the increase of T_x tends to decrease in the order of Fe > Co > Ni and no distinct change in T_x with Cu is seen for either the Al-Y-Cu or Al-La-Cu alloy.

The structural skeleton in the Al-based amorphous alloys is thought to consist mainly of Al-M and Al-R bonds with an attractive interaction. The equilibrium phase diagrams[24] of Al-M and Al-R alloys indicate the existence of a number of intermetallic compounds in their binary alloy systems. When the formation tendency and T_m of intermetallic compounds in Al-rich composition ranges corresponding to the glass-formation ranges in the Al-R-M system are compared with those in Al-R alloys, one notices that the minimum solute concentration for the

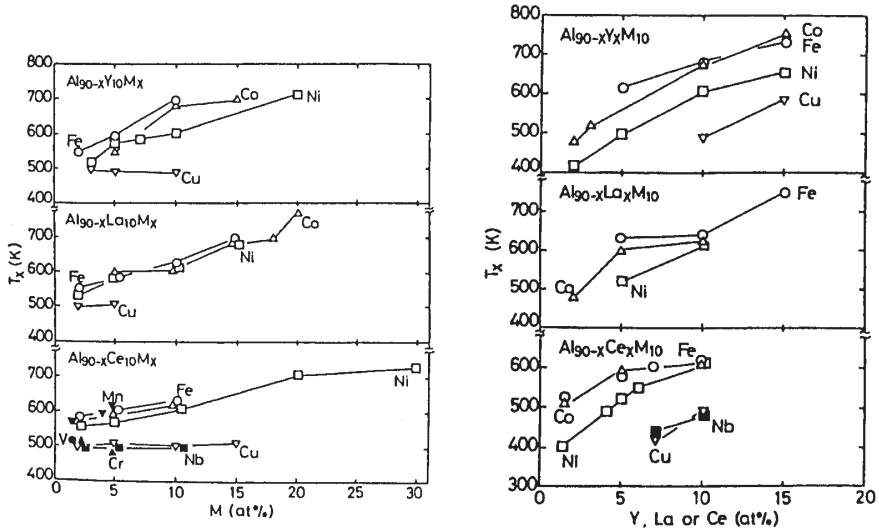

Fig. 6 Change in T_x as afunction of M (M=Fe, Co, Ni or Cu) concentration for $Al_{90-x}Y_{10}M_x$, $Al_{90-x}La_{10}M_x$, $Al_{90-x}Ce_{10}M_x$, $Al_{90-x}Y_xM_{10}$, $Al_{90-x}La_xM_{10}$ and $Al_{90-x}Ce_xM_{10}$ amorphous alloys.

formation of Al-rich compounds is 25 %Y (Al_3Y), 20 %La (Al_4La) and 20 %Ce (Al_4Ce) and the T_m of these compounds is considerably higher for Al_4(La or Ce) than for Al_3Y[24]. These differences suggest that the attractive interaction between Al and R atoms is considerably stronger for Al-La and Al-Ce atoms than for Al-Y atoms. This is presumably because the T_x values are higher for Al-La-M and Al-Ce-M amorphous alloys. On the basis of a similar concept that the degree of the attractive interaction between the constituent atoms exerts a significant effect on T_x, one can explain the result that T_x decreases in the order of Al-Fe-R > Al-Co-R > Al-Ni-R >> Al-Cu-R, because the T_x of Al-rich Al_3Fe, Al_9Co_2, Al_3Ni and Al_2Ce compounds decreases in the order of Fe > Co > Ni > Cu[24]. The good coincidence between T_x of the amorphous alloys and T_m of the Al-rich intermetallic compounds appears to support the appropriateness of the concept that the attractive interaction among the constituent elements contributes significantly to the glass formation of the metal-metal type amorphous alloys.

4.3 Mechanical Properties and Corrosion Resistance[27, 28]

The σ_f, E and H_v of the Al-Y-Ni, Al-La-Ni and Al-Ce-Ni amorphous alloys are summarized in Table 2, where the data of $\varepsilon_{t,f} = \sigma_f/E$ and $\varepsilon_{c,y} \fallingdotseq 9.8H_v/3$ are also shown for reference. The approximation of $\varepsilon_{t,f} \fallingdotseq 9.8H_v/3E$ is based on the fact that an amorphous alloy exhibits little work-hardening and thus the compressive yield strength is related by $\sigma_{c,y} \fallingdotseq 9.8H_v/3$[36]. As seen

Table 2 Mechanical properties of Al-Y-Ni, Al-La-Ni and Al-Ce-Ni amorphous alloys

Alloy (at%)	σ_f (MPa)	E (GPa)	H_v	$\varepsilon_{t,f} = \sigma_f/E$	$\varepsilon_{c,y} \approx 9.8H_v/3E$
$Al_{88}Y_2Ni_{10}$	920	71.0	340	0.013	0.016
$Al_{87}Y_8Ni_5$	1140	71.2	300	0.016	0.014
$Al_{87}La_8Ni_5$	1080	88.9	260	0.012	0.010
$Al_{84}La_6Ni_{10}$	1010	83.6	280	0.012	0.010
$Al_{86}Ce_4Ni_{10}$	810	54.6	300	0.015	0.018
$Al_{85}Ce_5Ni_{10}$	935	59.4	320	0.016	0.018

in the table, σ_f lies in the range of 920 to 1140 MPa for the Al-Y-Ni alloy, 1010 to 1080 MPa for the Al-La-Ni alloys, and 810 to 935 MPa for the Al-Ce-Ni alloys and is considerably higher for the Al-Y-Ni and Al-La-Ni alloys than for the Al-Ce-Ni alloys. No distinct compositional dependence of σ_f is seen for the three alloy systems, while E, H_v and $\sigma_{c,y}$ increase with decreasing Al content; from 52.4 to 84.2 GPa, 300 to 380 and 980 to 1240 MPa, respectively, for the Al-Y-Ni alloys; from 64.7 to 88.9 GPa, 260 to 320 and 850 to 1080 MPa, respectively, for the Al-La-Ni alloys; and from 53.2 to 60.3 GPa, 215 to 335 and 555 to 935 MPa, respectively, for the Al-Ce-Ni alloys. Thus, the properties except σ_f have a similar compositional dependence. Nonexistence of compositional dependence for σ_f has a similar compositional dependence. Nonexistence of compositional dependence for σ_f is presumably because σ_f is highly sensitive to the structure and smoothness of sample surface. In any event, it is notable that the $Al_{87}Y_8Ni_5$ and $Al_{87}La_8Ni_5$ amorphous alloys exhibit high static strengths of 1080 to 1140 MPa for σ_f and 260 to 300 for H_v which greatly exceed the highest values of 550 MPa and 180[29], respectively, for conventional Al-based crystalline alloys subjected to an optimum age-hardening treatment. The specific strength defined by the ratio of σ_f to density (ρ) is estimated to reach 38 for the $Al_{87}Y_8Ni_5$ alloy and 34 for the $Al_{87}La_8Ni_5$ alloy, which is higher than that (33) reported by Inoue et al.[30] for Ni-Si-B-Al amorphous wires with σ_f of about 2750 MPa. However, these values for σ_f/ρ are slightly lower than those (40-56) for Fe-Si-B[31] and Co-Si-B[32] amorphous wires with a high σ_f which ranges from 3000 to 3900 MPa.

We examined the fracture surface appearance of an $Al_{87}Y_8Ni_5$ amorphous ribbon fractured by uniaxial tensile test. The fracture surface consisted of a smooth region caused by shear sliding and a vein region caused by final catastrophic fracture after shear sliding. It has been reported by Masumoto and Maddin[26] that the fracture accompanying the shear sliding takes place along the shear plane declined by 45 to 55 degrees to the direction of the tensile load. A similar feature of the fracture surface appearance was also observed for the Al-La-Ni and Al-Ce-Ni amorphous ribbons. These features in the fracture behavior are also the same as those[33] reported previously for the other ductile amorphous alloys produced by liquid quenching. The similarity allows us to infer that the Al-based amorphous alloys have good ductility comparable to conventional ductile amorphous alloys.

The correlation between E and σ_f, H_v or T_x was also investigated for the Al-Y-Ni amorphous alloys. The three properties of σ_f, H_v and T_x tend to increase with increasing E. The correlation between E and σ_f or H_v was empirically expressed by the following approximate equations; $\varepsilon_{t,f}=\sigma_f/E$ 0.015 and $\varepsilon_{c,y}\fallingdotseq 9.8H_v/3E\fallingdotseq 0.017$. The $\varepsilon_{t,f}$ and $\varepsilon_{c,y}$ values are nearly equal to the respective values of 0.018 and 0.014[34] for the Fe-, Co-, Ni-, Pd-, Pt- and Cu-based amorphous alloy wires.

In addition, the Al-Y-Ni and Al-La-Ni amorphous alloys with high σ_f, i.e., above 1000 MPa, were found to exhibit high corrosion resistance in HCl and NaOH solutions which greatly exceed that of conventional Al-based crystalline alloys. As shown in Table 3, the corrosion losses of the Al-Y-Ni amorphous alloy in 1 N HCl and 0.25 N NaOH solutions at 293 K are 68 and 240 times, respectively, as small as those for the high-strength Al-Cu-Mg alloy subjected to an optimum heat treatment. It is particularly notable that the Al-based amorphous alloys have high corrosion resistance even in the alkline solution. This is in contrast to the fact that the solution has generally been used as a reagent for dissolving Al-based crystalline alloys. The discovery of the Al-Y-Ni and Al-La-Ni amorphous alloys exhibiting the high specific strength combined with good ductility and high corrosion resistance allows us to expect that the high-strength Al-based amorphous alloys will be valuable for applications in areas where these properties are required simultaneously.

4.4 Glass Transition Behavior[35]

Figure 7 shows the compositional dependence of the glass transition temperature (T_g) and T_x for amorphous Al-Y-Ni and Al-Ce-Ni alloys measured at a scanning rate of 0.67 K/s. In the figure, T_x is represented by an asterisk. It is seen that the glass transition phenomenon was observed prior to crystallization in the vicinity of 10 %Y for the Al-Y-Ni system and 6 %Ce for the Al-Ce-Ni system, indicating that the separation of glass transition from crystallization is mainly dominated by the Ln metals of Y and Ce and is independent of Ni content. T_g and T_x increase significantly with increasing solute concentration from 490 to 582 K and 518 to 604 K,

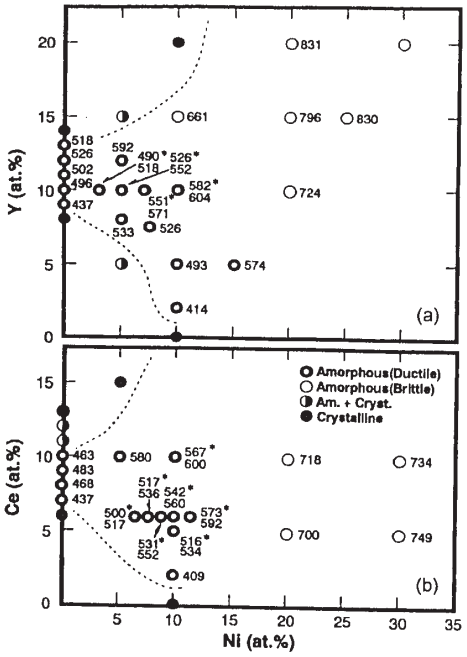

Fig. 7 Composition ranges for the formation of the amorphous phase, and the changes of T_g and T_x in (a) Al-Y-Ni and (b) Al-Ce-Ni systems. Double open circle, amorphous (ductile); open circle, amorphous (brittle); semi-open circle, amorphous plus crystalline; solid circle, crystalline. The asterisk represents t_g.

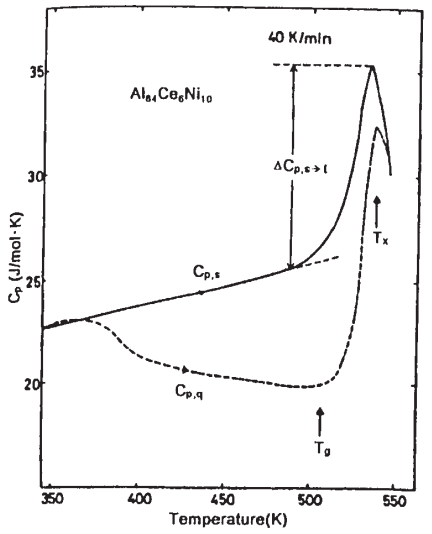

Fig. 8 The thermogram $C_{p,q}(T)$ of an amorphous $Al_{84}Ce_6Ni_{10}$ alloy in the as-quenched atate. The solid line represents the thermogram $C_{p,s}(T)$ of the sample heated to 520 K.

respectively, for the Al-Y-Ni alloys and from 500 to 573 K and 517 to 600 K, respectively, forthe Al-Ce-Ni alloys. In addition, Fig. 7 shows a general tendency that the amorphous alloys exhibiting a glass transition have a good bending ductility.

As an example, Fig. 8 shows the thermograms of an amorphous $Al_{84}Ce_6Ni_{10}$ alloy. The C_p value of the as-quenched phase is 22.8 J/mol-K near room temperature. As the temperature rises, the C_p value gradually increases initially and then begins to decrease at about 365 K, indicating an irreversible structural relaxation at about 365 K. With a further increase in temperature, the C_p value shows a minimum at about 500 K, then increases rapidly in the region of glass transition at about 515 K and reaches 32.4 J/mol-K for the supercooled liquid around 535 K. With further increasing temperature, the supercooled liquid begins to crystallize at 540 K. Figure 8 also shows that the amorphous alloys have a large difference, $\Delta C_{p,s\to l}$, in specific heat between the amorphous solid and supercooled liquid reaching 9.2 J/mol-K. The difference in $C_p(T)$ between the as-quenched and the reheated states, $[\Delta C_p(T)]$, manifests the irreversible structural relaxation which is presumed to arise from the annihilation of various kinds of quenched-in "defects" and the enhancement of the topological and chemical short-range ordering through the atomic rearrangement. The T_g and $\Delta C_{p,s\to l}$ as a function of Ni or Ce concentration were also examined for the Al-Y-Ni and Al-Ce-Ni amorphous alloys. The T_g increased almost linearly with increasing solute concentration, while the $\Delta C_{p,s\to l}$ values were the largest near the center of the compositional range where the amorphous alloys with a glass transition were obtained. Considering the general tendency[36] that the larger the $\Delta C_{p,s\to l}$ values the easier is the formation of an amorphous phase, it is expected that an amorphous phase with high structural

stability is obtained in the vicinity of $Al_{83}Y_{10}Ni_7$ and $Al_{84}Ce_6Ni_{10}$. Thus, the Al content of stable amorphous alloys with the largest $\Delta C_{p,s\rightarrow l}$ is nearly equal in the two alloys, but the ratios of Y or Ce to Ni are significantly different.

An elongation curve of an amorphous $Al_{85}Y_{10}Ni_5$ alloy was measured under an initial tensile stress of 0.98 MPa at a heating rate of 0.17 K/s. The length of the specimen begins to increase at about 320 K and increases gradually up to about 520 K and then rapidly in the range from 530 to 560 K. With a further increase in temperature, the increase in the length stops suddenly due to crystallization. The elongation curve before crystallization was divided into two stages corresponding to an amorphous solid and a supercooled liquid and each coefficient of thermal expansion (α) was 3.8×10^{-5} K^{-1} for the amorphous solid in the range of 320 to 520 K (stage-I) and 100×10^{-5} K^{-1} for the supercooled liquid in the range of 530 to 560 K (stage-II). The extraordinarily high α value for the supercooled liquid is due to a much lower viscosity.

Based on the data of elongation, the viscosities (η) as a function of temperature were evaluated for amorphous $Al_{85}Y_{10}Ni_5$ and $Al_{84}Ce_6Ni_{10}$ alloys. Figure 9 plots the η values as a function of reciprocal temperature. The η values of the Al-based alloys decrease significantly from 2×10^{14} Pa.s (2×10^{15} poise) at 488 K to 3×10^{12} Pa.s at 521 K, and no distinct difference in η (T) is seen for the two amorphous alloys. It is notable that the η value (3×10^{12} Pa.s) at 521 K is nearly equal to 10^{12} Pa.s which has been thought[36] to be the viscosity for a supercooled liquid near T_g. This indicates that the amorphous solid heated at 521 K changes to a nearly equilibrium supercooled liquid state.

It is generally known that the glass transition gives rise to significant changes of E, σ_f and deformation behavior, in addition to the above-described changes in specific heat and viscosity. It is of importance for the present Al-based amorphous alloys to clarify the changes in E, σ_f, elongation and fracture behavior by the transition from amorphous solid to supercooled liquid. Figure 10 shows the temperature dependence of σ_f, ε_f and E for the $Al_{85}Y_{10}Ni_5$ and $Al_{84}Ce_6Ni_{10}$ amorphous alloys. With increasing temperature, the σ_f and E values gradually decrease from 920 to 700 MPa and 72.6 to 55.0 GPa, respectively, in the amorphous solid and rapidly to 100 MPa and 21.6 GPa, respectively, in the supercooled liquid and then increases steeply upon crystallization. On the other hand, the ε_f steeply increases

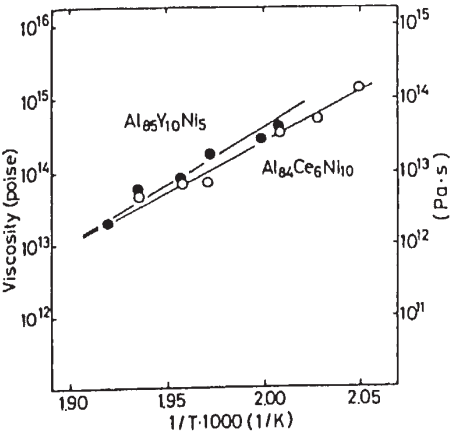

Fig. 9 Change in viscosity of amorphous $Al_{85}Y_{10}Ni_5$ and $Al_{84}Ce_6Ni_{10}$ alloy as a function of reciprocal temperature.

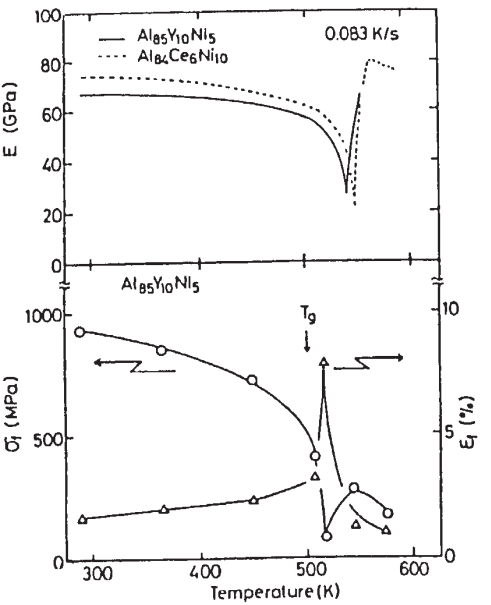

Fig. 10 Changes in E, σ_f and tensile fracture strain (ε_f) of amorphous $Al_{85}Y_{10}Ni_5$ and $Al_{84}Ce_6Ni_{10}$ alloys as a function of testing temperature.

to 8 % in the vicinity of glass transition, followed by a significant decrease of ε_f by crystallization. The amorphous $Al_{85}Y_{10}Ni_5$ alloy tested at 508 K near the glass transition is subjected to a sever homogeneous necking which appears to have taken place through a viscous flow mechanism. The feature of deformation and fracture behaviors agrees with that[26] for Pd-based amorphous alloys exhibiting the glass transition phenomenon.

5. TRIALS TO PRODUCE BULK AMORPHOUS Al-BASED ALLOYS[37]

The production of Al-Ni-Y amorphous powders was tried by high-pressure helium atomization. The resulting $Al_{85}Y_{10}Ni_5$ powder has a spherical shape. The surface is very smooth and no grain boundary is seen. The X-ray diffraction pattern of the -25 μm powder consisted of broad diffraction peaks, indicating the formation of a mostly single amorphous phase. With further increasing powder diameter, the structure is composed of amorphous and crystalline phases for the 25-37 μm fraction and a crystalline phase for the powder with a size fraction above 37 μm. In addition, the size fraction of the amorphous Al-Y-Ni powder was measured by the microtrac analysis method. The fraction is 41 % for the powder below 10 μm in size, followed by 24 % for the powder between 10 and 15 μm in size, 25 % for the 15 to 21 μm powder and 11 % for the powder above 21 μm in size. It is thus notable that the powder below 15 μm in size was prepared with a high yield fraction of 65 %. Furthermore, the DSC curve obtained from the $Al_{85}Y_{10}Ni_5$ amorphous powder was confirmed to be the same as that for the melt-spun amorphous ribbon, and no appreciable difference in T_g and T_x was seen by Inoue et al.[38]. It is therefore concluded that the amorphous powder produced by high-pressure helium atomization can be used as a raw material to produce an amorphous bulk by consolidation at temperatures near T_g.

The extrusion of the $Al_{85}Y_{10}Ni_5$ amorphous powder into an amorphous bulk at extrusion ratios of four and seven was tried by changing the extrusion temperature. The extruded bulk was obtained at temperatures above 543 K and the relative density was measured to be 0.969 at 543 K, 0.980 at 573 K, 0.987 at 603 K and 0.996 at 673 K. The structure of the extruded bulk consists of a mostly amorphous phase at 543 K, coexisting amorphous + Al phases at 573 K, coexisting amorphous + Al + unidentified compound at 603 K and Al + compound at 673 K.

We measured the compressive stress-strain curves of $Al_{85}Y_{10}Ni_5$ bulk samples with high densities above 98 %, extruded at 603 and 673 K, along with the data[39] of a conventional high-strength Al-based crystalline alloy (2017). It is notable that the bulk consisting of amorphous and Al exhibits a high compressive fracture strength ($\sigma_{c,f}$) reaching 1470 MPa nd an E of 145 GPa, although no appreciable plastic elongation is seen. The increase of the extruded temperature to 673 K results in a decrease of the yield (0.2 % proof) stress to 1220 MPa and E to 120 GPa, and an increase of plastic elongation to 0.6 %, though the $\sigma_{c,y}$ remains unchanged. It is to be noticed that the $\sigma_{c,f}$ and E for the bulk material with a mixed structure of amorphous and fcc phases are about 2 to 3 times as large as those (450 MPa and 71 GPa)[39] for the optimumly aged 2017 alloy. The extremely high $\sigma_{c,f}$ which exceeds the tensile fracture strength ($\sigma_{t,f} \fallingdotseq$ 1140 MPa) of the $Al_{85}Y_{10}Ni_5$ amorphous ribbon is presumably due to a dispersion-hardening resulting from a homogeneous dispersion of the spherical Al phase with a size of about 30 nm in an amorphous matrix.

The high-temperature hardness of the high-strength $Al_{85}Y_{10}Ni_5$ bulk samples consisting of a mostly amorphous phase or coexisting amorphous + Al phases was measured as a function of testing temperature. The heating rate to each testing temperature was 10 K/min and the sample was kept fo 10 min at each testing temperature. The H_v at room temperature is 340 for the amorphous bulk extruded at 543 K and 405 for the amorphous + Al bulk extruded at 603 K, being about three times as high as that (145)[39] for the 2017 alloy. Furthermore, the high hardness of 150 at 573 K is obtained for the bulk sample extruded at 603 K. It is thus concluded that the extruded bulk materials have high heat-resistant hardness as well as high $\sigma_{c,f}$ and E values. The good mechanical strengths allow us to expect that the extruded bulk samples may be used as a high-strength material with low density under a compressive stress condition.

As described above, it is very difficult to produce an amorphous bulk alloy without crystallinity by extrusion of the amorphous alloy powders, when the powders were once exposed in air and coated with an oxide layer. The difficulty is due to the preparation of a true bonding between their powders because the surface oxide film cannot be eliminated during warm extrusion at the temeperature near T_g. This result also indicates the possibility that the suppression of the surface oxide layer on the powder enables the production of a bulk amorphous

alloy even in the same extrusion condition. With the aim of suppressing the formation of the surface oxide film, we have developed a new closed system in which the production of amorphous alloy powder by gas atomization, followed by the sieving, precompaction and canning and sealing into a copper tube can be made in a well-controlled atmosphere with an oxide or a moisture concentration below 1 ppm, as illustrated in Fig. 11. We have confirmed that the use of the closed P/M processing system can produce amorphous powders with the same oxygen content as that for the master alloy. By extruding the amorphous powders prepared in the closed system at the temperature near T_g and an extrusion ratio of 4, a consolidated bulk amorphous alloy was produced in the case where the core material is set in the central part of extruding die. Figure 21 shows an X-ray diffraction pattern of the extruded bulk $Al_{85}Ni_{10}Y_5$ alloy, together with the data on the as-atomized amorphous powder. The diffraction pattern consists only of a broad peak and no appreciable diffraction peak due to crystallization is seen for both samples. The tensile strength of the extruded bulk amorphous alloy was measured to be 900 MPa which is slightly lower than that (1050 MPa) for the corresponding melt-spun amorphous alloy ribbon. Figure 12 (a) and (b) show the tensile fracture surface appearance of the extruded bulk allloys made from amorphous alloy powders prepared in the closed and open systems, respectively. That is, although a distinct interparticle fracture takes place for the bulk alloy prepared from the powder in the open system, the bulk amorphous alloy made from the powder prepared in the closed system consists mainly of a well-developed vein pattern and no appreciable interparticle fracture mode is seen over the fracture surface. The transgranular fracture mode for the bulk amorphous alloy made from the clean powders indicates clearly that the bonding among the powders is in a truely tight state. It is therefore concluded that the suppression of the oxide surface layer on the atomized powders is important for the production of a bulk amorphous alloy by the powder metallurgy technique. Even by the use of the clean amorphous powder, it is difficult to produce a bulk amorphous alloy with the same high

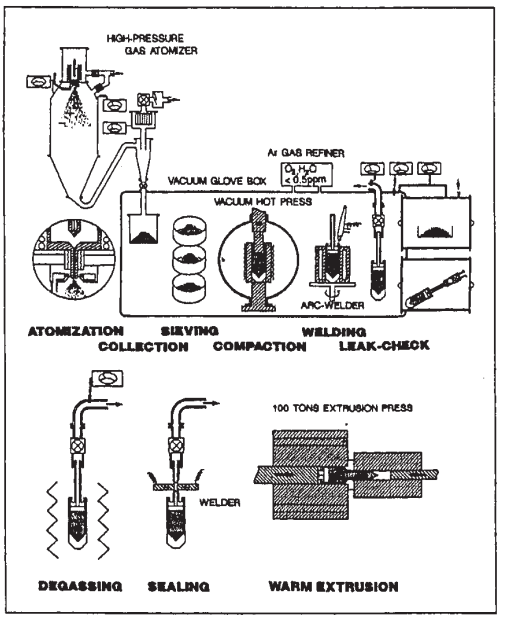

Fig. 11 Closed P/M processing system devel oped for the production and consolidation of amorphous alloy powders-schematic.

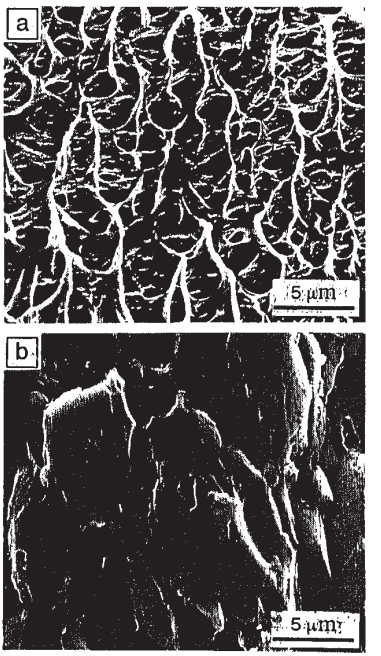

Fig. 12 Fracture surface appearances of $Al_{85}Ni_{10}Mm_5$ amorphous alloy compacts produced through the closed (a) and open (b) P/M processings

tensile strength in the case where the core material is not used. The difficulty is due to the partial crystallization resulting from the increase in sample temperature with increasing extrusion ratio. This result suggests that the formation of a bulk amorphous alloy with the same σ_f as that for the melt-spun amrphous alloy ribbons is possible only for an amorphous alloy with a much larger temperature interval of the supercooled liquid region defined by the difference between T_g and T_x. This presumption has presently been confirmed for the extruded bulk amorphous alloy made from Zr-Al-Ni-Cu amorphous alloy powders with the temperature interval of about 100 K.

6. PRODUCTION AND MECHANICAL PROPERTIES OF BULK NANOCRYSTALLINE Al-BASED ALLOYS AND THEIR APPLICATIONS

Amorphous alloy powders in Al-Y-Ni and Al-Ce-Ni systems have been produced[38] by gas atomization with applied pressure of 4 to 10 MPa. Although the formation of their amorphous powders is limited to the particle size fraction below 25 μm, the weight ratio is as high as 85 %. Thus, it is concluded that Al-based amorphous powders can be obtained at high production ratios.

The warm extrusion of the Al-based amorphous powders was made over a wide temperature (T_e) range of 500-783 K[37,40]. For instance, the warm extrusion of an $Al_{85}Y_{10}Ni_5$ amorphous powder was possible at temperatures above 540 K. The packing density was 97 % at T_e=543 K. With increasing T_e, the density increases and reaches about 100 % at T_e above 673 K. The structure of the extruded alloy consists of an amorphous single phase at 543 and 573 K, a duplex structure of amorphous and Al phases at 603 K and mixed phases of Al + Al_3Y + Al_3Ni above 673 K. The $\sigma_{c,f}$ and E of the extruded alloy consisting of amophous and Al phases are 1470 MPa and 145 GPa, respectively, which are two to three times higher than those ($\sigma_{c,y}$=450 MPa, E=71 GPa)[39] of the conventional 2017 aluminum alloy. As T_e rises to 673 K, $\sigma_{c,f}$ and E decrease to 1220 MPa and 121 GPa, accompanying the appearance of plastic elongation of 0.5-1.0 %. The $\sigma_{c,f}$ value of the extruded alloy is higher than that (σ_f=1140 MPa) of a melt-spun $Al_{85}Y_{10}Ni_5$ amorphous ribbon. The increase in $\sigma_{c,f}$ is thought to orginate from the dispersion strengthening caused by the homogeneous dispersion of nanoscale Al particles with a size of about 30 nm in the amorphous matrix.

As described above, although the compressive strength of the $Al_{85}Y_{10}Ni_5$ alloy consolidated at temperatures below 673 K is high, the σ_f shows lower values ranging from 500 to 700 MPa. Consolidation at temperatures above 703 K was carried out with the aim of increasing σ_f. The $Al_{85}Y_{10}Ni_5$ alloy extruded at 783 K has a mixed structure consisting of dispersed Al_3Y and Al_3Ni compounds with a size of about 50 nm in the Al matrix with a grain size of about 0.1 μm. Judging from the previous result[41] that the grain size of a metastable Al-based solid solution in a rapidly solidified $Al_{95}Ce_3Fe_2$ alloy is about 2 μm, it is concluded that the present process consisting of warm extrusion of the amorphous powders is useful for the formation of the ultrafine mixed structure consisting of fine Al_3Ni and Al_3Y particles embedded in the Al matrix. Figure 13 shows the temperature dependence of σ_f, E, $\varepsilon_{t,p}$ and H_v of the $Al_{85}Y_{7.5}Ni_{7.5}$ and $Al_{91}Y_{4.8}Ni_3Co_{1.2}$ alloys along with the data[39] of Vasudevan and Doherty for the commercial 2014-T6 and 7075-T6 alloys. The σ_f,

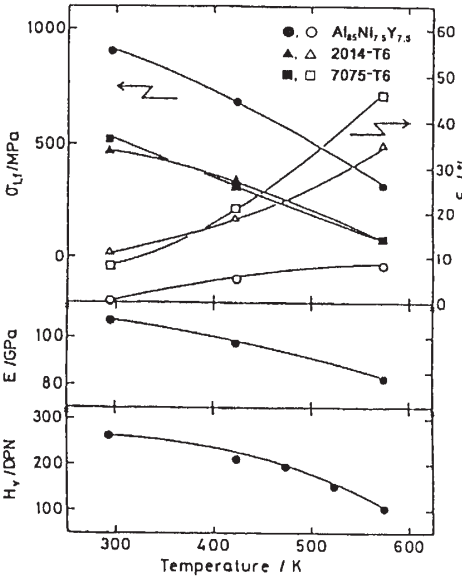

Fig. 13 Changes in mechanical properties with temperature for an $Al_{85}Ni_{7.5}Y_{7.5}$ bulk produced by extrusion at 783 K and an extrusion ratio of 12.

E, $\varepsilon_{t,p}$ and H_v values at room temperature are 940 MPa, 115 GPa, 2.0 % and 265, respectively, for the former alloy and 800 MPa, 84 GPa, 3.5 % and 220, respectively, for the latter alloy. Although these values decrease with increasing temperature, the high strength level of σ_f=380 MPa, E=85 GPa and H_v=105 is kept at 573 K. It is interesting that these values are about twice as high as those for commercial Al-based alloys. On the other hand, the $\varepsilon_{t,p}$ increases with increasing temperature and is about 10 % at 573 K.

The stability of the high σ_f values against annealing is also shown for the bulk $Al_{88.5}Ni_8Mm_{3.5}$ (Mm=mischmetal) alloy extruded at 633 K in Fig. 14[42, 43], in comparison with the data of Vasudevan and Doherty[39], for the A7075 alloy. The open and closed circles in the figure represent the data after annealing at each temperature for 1 and 100 h, respectively. σ_f in the case of 1 h annealing for the extruded Al-Ni-Mm bulk is as high as 940 MPa at room temperature which is much higher than that (700 MPa)[39] for the A7075 alloy. Although σ_f decreases monotonously with increasing temperature, it maintains rather high values of 700 MPa at 423 K and 520 MPa at 473 K. It should be noticed that no appreciable decrease in σ_f is seen even after annealing for 100 h, although the σ_f of the A7075 alloy decreases by 5 % at 423 K and by 45 % at 473 K. Consequently, in addition to the high tensile strength, the Al-Ni-Mm alloy also has a good heat resistance of the tensile strength. The Young's modulus of the extruded Al-Ni-Mm alloy was also as high as 91 GPa. The achievement of the extremely high σ_f has been attributed to the formation of a mixed structure consisting of homogeneously dispersed Al_3Ni and $Al_{11}(La, Ce)_3$ compounds with a size of 50 nm in an Al matrix with a grain size of 100-200 nm, as shown in Fig. 15. Furthermore, the high σ_f has been roughly evaluated by Ohtera et al.[42] from the sum of the dispersion strengthening and the strengthening due to grain size refinement, as shown in Fig. 16. Such a finely mixed structure cannot be obtained by conventional thermomechanical treatments. The good heat resistance of σ_f for the present alloy is presumably because the strength mechanism is due to the dispersion hardening by the intermetallic compounds, which is different from the result[39] that the strengthening mechanism for the A7075 alloy is due to the age-hardening mechanism.

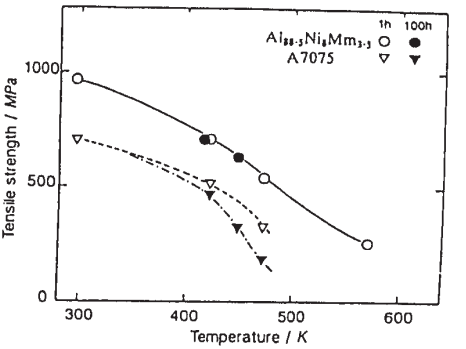

Fig. 14 Temperature dependence of tensile strength for as-extruded bulk $Al_{88.5}Ni_8Mm_{3.5}$ annealed for 1 h and 100 h at each testing temperature. The data for the A7075 alloy are also shown for comparison.

Fig. 15 Bright-field electron micrograph of an as-extruded $Al_{88.5}Ni_8Mm_{3.5}$ alloy.

The fatigue limit after the cycles of 10^7 for the extruded Al-Ni-Mm alloy was measured to be 330 MPa at 293 K and 196 MPa at 473 K. In orde to compare the present fatigue limit with the data for other Al-based alloys, we plot the fatigue limit against the tensile strength for Al-based alloys in Fig. 17. It is seen that the fatigue limit is about 1.3 times as high as the highest fatigue limit (260 MPa)[39] reported for newly developed Al-based alloys made from rapidly solidified powders. It is therefore concluded that both the σ_f and fatigue limit for the extruded Al-Ni-Mm alloy are much superior to those for the newly commercialized Al-based

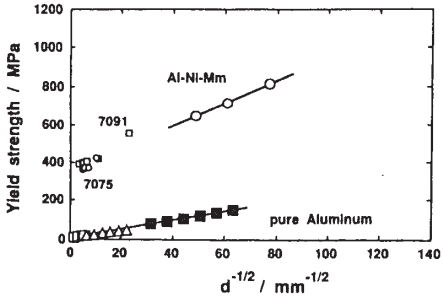

Fig. 16 Hall-Petch relation of the yield strength ($\sigma_{0.2}$) at room temperature for as-extruded $Al_{88.5}Ni_8mm_{3.5}$ alloys.

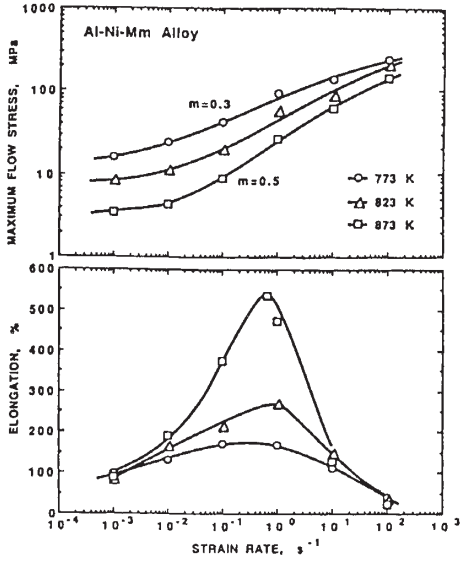

Fig. 18 Variation of (top) flow stress and (bottom) elongation for as-extruded $Al_{88.5}Ni_8Mm_{3.5}$ alloys as a function of strain rate at temperatures between 773 and 873 K.

alloys developed by using the powder metallurgy technique as well as the conventional Al-based alloys.

It is also expected that a low coefficient of thermal expansion and a high wear resistance are also obtained for the Al-Ni-Mm alloy because of the precipitation of a large amount of Al_3Ni and $Al_{11}(La, Ce)_3$ compounds. The

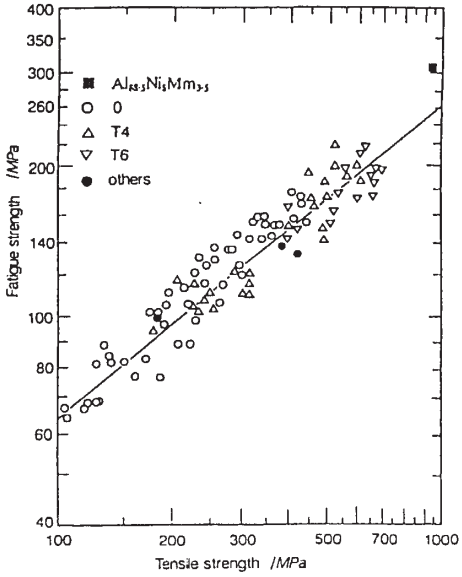

Fig. 17 Relation between fatigue limit after the cycles of 10^7 and tensile fracture strength for an as-extruded $Al_{88.5}Ni_8Mm_{3.5}$ alloy. The data for conventional Al-based alloys are also shown for comparison. The symbols O, T4 and T6 represent the samples that were subjected to annealing, natural aging after solid solutioning and artificial aging after solid solutioning, respectively.

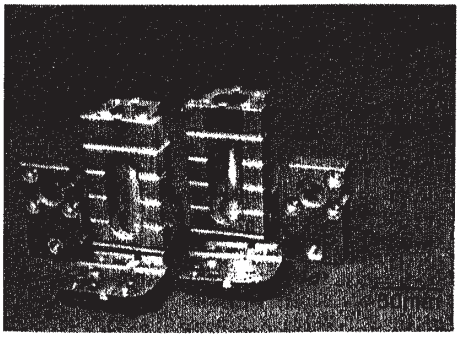

Fig. 19 Machinery parts made from $Al_{88.5}Ni_8Mm_{3.5}$ powders were produced by extrusion, forging and mechanical polishing.

coefficient of thermal expansion (α) in the temperature range of 423-473 K and the relative wear resistance against S45C were examined in comparison with the data[39] for the A6061 and A5056 alloys. The α value is about 20 % smaller than that for the conventional Al-based alloys. The wear loss is also about 25 % smaller than that for the Al-Si-Mg and Al-Mg base alloys. It is thus cocnluded that the Al-Ni-Mm alloy has a high wear resistance as well as a low α value.

In addition to the good mechanical properties resulting from the finely mixed structure, the bulk alloys have been reported[44, 45] to exhibit marked superplasticity in a high strain rate range of 0.1-10 s^{-1}, as shown in Fig. 18, in which the strain rate sensitivity exponent (m value) is above 0.5 and the maximum elongation reaches as large as 550 % at a strain rate of about 1.0 s^{-1}.

By utilizing the good superplasticity, the present mixed phase alloys have been deformed into machinery parts with various complicated morphologies. The bulk Al-Ni-Mm alloys produced by the process of extrusion, forging and mechanical polishing have been used[46] as machine parts that are required to have simultaneously high σ_f, high fatigue limit and low α, as exemplified in Fig. 19. In addition to such machine parts, the new Al-based alloys produced by extrusion of amorphous powders are expected to be used in various application fields where the simultaneous achievement of high strength with light weight, high heat resistance of strength, high fatigue strength, low α and wear resistance is required.

REFERENCES

1. W. Klement. R.H. Wilens and P. Duwez: Nature, 187(1960), 869.
2. Amorphous Metallic Alloys, ed. by F.E. Luborsky, Butterworths, London (1983).
3. H.S. Chen: Rep. Prog. Phys., 43(1980), 353.
4. Rapidly Solidifiied Alloys, ed. Howard H. Liebermann, Marcel Dekker, New York (1993).
5. R.B. Schwarz: Rapidly Solidiifed Alloys, ed. Howard H. Liebermann, Marcel Dekker, New York (1993), p. 157.
6. Y. Kawamura, H. Kato, A. Inoue and T. Masumoto: Int. J. Powder Metall., 33/2(1997), 50.
7. A. Inoue: Met. Trans., 36(1995) 866.
8. A. Inoue: Mater. Sci. Forum, 179-181(1995), 691.
9. A. Inoue: Mater. Sci. Eng., A226-228(1997), 357.
10. P. Predecki, B.C. Giessen and N.J. Grant: Trans. Metall. Soc. AIME, 233(1965), 1438.
11. R. Ramachandrarao, M. Laridjani and R.W. Cahn: Z. Metallkd., 63(1972), 43.
12. H.A. Davies and J.B. Hull: Scr. Metall., 6(1972), 241.
13. K. Chattopadyay, R. Ramachandrarao, S. Lele and T.R. Anantharaman: Proc. 2nd Int. Conf. on Rapidly Quenched Metals, eds N.J. Grant and B.C. Giessen, MIT Press, Cambridge, (1976), p. 157.
14. P. Furrer and H. Warlimont: Mater. Sci. Eng., 28(1977), 127.
15. G.V.S. Sastry, C. Suryanarayana, O.N. Srivastava and H.A. Davies: Trans. Indian Inst. Met., 31(1978), 292.
16. A. Inoue, A. Kitamura and T. Masumoto: J. Mater. Sci., 16(1981), 1895.
17. R. O. Suzuki, Y. Komatsu, K. F. Kobayashi and P.H. Shingu: J. Mat. Sci., 18(1983), 1195.
18. A. Inoue, M. Yamamoto, H.M. Kimura and T. Masumoto: J. Mater. Sci. Lett., 6(1987), 194.
19. A.P. Tsai, A. Inoue and T. Masumoto: Met. Trans., 19A(1988), 1369.
20. A. Inoue, K. Ohtera, A.P. Tsai and T. Masumoto: Jpn. J. Appl. Phys., 27(1988), L280.
21. A. Inoue, K. Ohtera and T. Masumoto: Jpn. J. Appl. Phys., 27(1988), L736.
22. A.P. Tsai, A. Inoue and T. Masumoto: Met. Trans., 19A(1988), 391.
23. H.A. Davies: Amorphous Metallic Alloys, ed F.E. Luborsky, Butterworths, London, (1983), p. 8.
24. T.B. Massalski: Binary Alloy Phase Diagrams, American Society for Metals, Ohio (1986).
25. H.S. Chen, J.T. Krause and E. Coleman: J. Non-Cryst. Solids, 78(1975), 157.
26. T. Masumoto and R. Maddin: Acta Met., 19(1971), 725.
27. A. Inoue, K. Ohtera, A.P. Tsai and T. Masumoto: Jpn. J. Appl. Phys., 27(1988), L479.
28. A. Inoue, K. Ohetera, A.P. Tsai and T. Masumoto: Proc. MRS Int. Meeting on Advanced Materials, Vol. 3, eds. M. Doyama, S. Somiya and R.P.H. Chang, MRS, Pittsbirgh (1989), p. 411.
29. Metals Databook, ed. Japan Inst. Metals, Maruzen, Tokyo (1983), p. 175.
30. A. Inoue, S. Furukawa, M. Higiwara and T. Masumoto: Metall. Trans., 18A(1987), 621.